THE JOURNAL OF BIOLOGICAL CHEMISTRY VOL. 286, NO. 40, pp. 34761–34769, October 7, 2011
Printed in the U.S.A.

Invasion of *Cryptococcus neoformans* into Human Brain Microvascular Endothelial Cells Is Mediated through the Lipid Rafts-Endocytic Pathway via the Dual Specificity Tyrosine Phosphorylation-regulated Kinase 3 (DYRK3)*[S]

Received for publication, January 12, 2011, and in revised form, June 20, 2011 Published, JBC Papers in Press, June 21, 2011, DOI 10.1074/jbc.M111.219378

Sheng-He Huang[‡1], Min Long[‡1], Chun-Hua Wu[‡], Kyung J. Kwon-Chung[§2], Yun C. Chang[§2], Feng Chi[‡], Susan Lee[¶], and Ambrose Jong[‡3]

From the Saban Research Institute, Children's Hospital Los Angeles, Departments of [‡]Pediatrics and [¶]Pathology, Keck School of Medicine, University of Southern California, Los Angeles, California 90027 and the [§]Laboratory of Clinical Infectious Diseases, NIAID, National Institutes of Health, Bethesda, Maryland 20892

Cryptococcus neoformans **is a neurotropic fungal pathogen, which provokes the onset of devastating meningoencephalitis. We used human brain microvascular endothelial cells (HBMEC) as the *in vitro* model to investigate how *C. neoformans* traverses across the blood-brain barrier. In this study, we present several lines of evidence indicating that *C. neoformans* invasion is mediated through the endocytic pathway via lipid rafts. Human CD44 molecules from lipid rafts can directly interact with hyaluronic acid, the *C. neoformans* ligand. Bikunin, which perturbs CD44 function in the lipid raft, can block *C. neoformans* adhesion and invasion of HBMEC. The lipid raft marker, ganglioside GM1, co-localizes with CD44 on the plasma membrane, and *C. neoformans* cells can adhere to the host cell in areas where GM1 is enriched. These findings suggest that *C. neoformans* entry takes place on the lipid rafts. Upon *C. neoformans* engagement, GM1 is internalized through vesicular structures to the nuclear membrane. This endocytic redistribution process is abolished by cytochalasin D, nocodazole, or anti-DYRK3 (dual specificity tyrosine-phosphorylation-regulated kinase 3) siRNA. Concomitantly, the knockdown of DYRK3 significantly reduces *C. neoformans* invasion across the HBMEC monolayer *in vitro*. Our data demonstrate that the lipid raft-dependent endocytosis process mediates *C. neoformans* internalization into HBMEC and that the CD44 protein of the hosts, cytoskeleton, and intracellular kinase-DYRK3 are involved in this process.**

Cryptococcus neoformans is the etiologic agent of cryptococcosis, which occurs primarily in immune-compromised hosts and occasionally occurs in normal hosts (1). It is an environmental yeast that initiates infection after inhalation and can disseminate hematogenously to almost every organ. If developed into cryptococcal meningoencephalitis, it is fatal unless treated; and even with treatment the fatality rate is close to 25%. In particular, an infection of the brain and meninges is the most common clinical manifestation of cryptococcosis as well as the most common cause of death from the disease (1, 2). Cryptococcosis becomes one of the most notorious HIV-associated opportunistic infections (3) Annually, close to 1 million cases of cryptococcal meningoencephalitis occur globally, resulting in about 700,000 deaths per year. It is generally accepted that the *C. neoformans* capsule is the major virulent factor of this pathogen (4).

To cause meningoencephalitis, *C. neoformans* must penetrate through the blood-brain barrier and migrate to the brain cortex. The blood-brain barrier mainly consists of brain microvascular endothelial cells (BMEC)[4] (5). One significant feature of BMEC is their ability to form tight junctions among the endothelial cells. Because of the high density of microvessels inside the brain, it is conceivable that BMEC is the primary site for *C. neoformans* brain invasion.

To determine how *C. neoformans* invades the brain, we have developed an *in vitro* blood-brain barrier model to investigate the interaction between *C. neoformans* and human BMEC (HBMEC). We have previously demonstrated that the *C. neoformans CPS1* gene encodes a hyaluronic acid synthase, and its product hyaluronic acid is an adhesion molecule that binds to HBMEC (6, 7). Further studies have revealed that CD44 of HBMEC functions as the primary receptor during *C. neoformans* invasion (8). In addition, *C. neoformans* infection of HBMEC induces the activation of PKCα (9). Perturbation of the function of PKCα subsequently reduces actin filament activity, suggesting that actin is a downstream effector of PKCα. Upon the interaction between *C. neoformans* and HBMEC, a subpopulation of CD44 and actin is translocated to the membrane rafts of the host (8). The dynamic interactions between *C. neoformans* hyaluronic acid and the host CD44 may represent an early adhesion step of *C. neoformans* on the HBMEC membrane lipid rafts. However, the molecular events at the *C. neoformans* entry site and the mechanism(s) of *C. neoformans* internalization are unknown.

* This work was supported, in whole or in part, by National Institutes of Health Grants R01-NS047599 (to A. J.) and R01-AI40635 from USPHS (to S. H. H.).

[S] The on-line version of this article (available at http://www.jbc.org) contains supplemental Figs. S1 and S2.

[1] Both authors contributed equally to this work.

[2] Supported by National Institutes of Health grants from the intramural program of NIAID.

[3] To whom correspondence should be addressed: Division of Hematology-Oncology, Mailstop 57, 4650 Sunset Blvd., Los Angeles, CA 90027. Tel.: 323-361-5647; Fax: 323-361-6114; E-mail: ajong@chla.usc.edu.

[4] The abbreviations used are: BMEC, brain microvascular endothelial cells; CTxB, cholera toxin subunit B; HBMEC, human BMEC.

Endocytosis is a multistep procedure that allows the cells to internalize macromolecules and particles into transport vesicles derived from the plasma membrane (10–12). Several endocytosis pathways are commonly observed in different cell types. It could be a caveolae-dependent, clathrin-dependent, phagocytosis, pinocytosis, or macropinocytosis event. In most cases, endocytosis is a lipid raft-mediated process. The lipid raft is a biochemically defined frame, not an organelle, and is also known as detergent-resistant membrane or detergent-insoluble glycolipid-rich membrane. The lipid rafts are enriched in cholesterol, glycosphingolipids, and sphingomyelin phospholipids with long, unsaturated acyl chains, glycosylphosphatidylinositol-linked proteins, and some membrane-spanning proteins (13). One important feature of membrane rafts is their highly dynamic nature, which allows the transient formation of membrane platforms to build up cell signaling complexes, as well as its participation in membrane trafficking (14). The involvement of lipid rafts in pathogen entry has been described for viruses and bacteria (15–17). For example, SV40 and HIV use lipid rafts for invasion (18, 19). The level of involvement of rafts in organism invasion is generally dependent on the concentration of raft-associated lipids and/or proteins at pathogen entry sites. Interestingly, our understanding on the many functions of lipid rafts in mammalian cells is derived from the behavior of interacting pathogens (20, 21). A number of pathogenic bacteria (22) and viruses (20) bind to order-preferring proteins and lipids on the surface of mammalian cells and appear to co-opt the host cell rafts during infection. For instance, cholera toxin B subunit (CTxB) binds to the lipid raft-enriched ganglioside GM1 (22, 23) and is internalized into mammalian cells, suggesting a role for rafts in normal endocytic pathways. CTxB has become a commonly used reagent for the studies of lipid raft dynamics.

Members of the DYRK (dual specificity tyrosine phosphorylation-regulated kinase) gene family catalyze the phosphorylation of both serine/threonine and tyrosine residues (24, 25). In general, DYRKs play key roles in cell proliferation, survival, and development. Although the members of this family share structural similarity, they differ in their substrate specificity suggesting their involvement in different cellular functions. Of the seven mammalian DYRK isoforms reported, only the DYRK1A gene and its products have been well characterized (25). One member, DYRK3, is initially identified as an erythroid kinase (REDK), as the gene is expressed preferentially in erythroid cells (26). Antisense REDK oligonucleotides promote erythroid colony formation by human bone marrow cells, without affecting the numbers of colony-forming unit (CFU)-GM, CFU-G, or CFU-GEMM (26). The results suggested that DYRK3 exerts an inhibitory role during a CFU stage of erythroid development. Studies in DYRK3 knock-out transgenic mice have revealed that erythropoiesis is increased during anemia, suggesting that DYRK3 attenuates red cell production during anemia (27). The functions of DYRK3 may also be associated with cAMP-dependent protein kinase (PKA) as well as cyclic AMP-response element-binding protein pathways (28). However, the exact *in vivo* function of DYRK3 is ambiguous. More recently, a genome-wide screening of human kinases has determined that DYRK3 is required for ganglioside GM1 redistribution via the endocytic pathway, upon SV40 infection in HeLa cells (29). The knockdown of DYRK3 results in an accumulation of enlarged vesicular structures inside the cytosol, suggesting a perturbation of the endocytic pathway (29).

In this study, we demonstrate that the *C. neoformans* receptor, CD44, is associated with ganglioside GM1, a lipid raft marker, and that *C. neoformans* elicits a significant redistribution of GM1, eventually surrounding the nuclear membrane. This dynamic change can be disturbed by cytochalasin D, nocodazole, and anti-DYRK3 siRNA. We further demonstrate that DYRK3 is involved in *C. neoformans* invasion. Our results suggest that *C. neoformans* utilizes the endocytic signaling pathway in HBMEC to traverse across the blood-brain barrier.

EXPERIMENTAL PROCEDURES

Strains, Media, and Cultures—C. neoformans strains B-4500FO2 and C1186 were used in this study (6, 7). C1186 was derived from B-4500FO2 and stably expresses GFP. Yeast cells were grown aerobically at 30 °C in 1% yeast extract, 2% peptone. and 2% dextrose (YPD broth) (Difco). Cells were harvested at early log phase, washed with phosphate-buffered saline (PBS) for immunofluorescence microscopic studies, or resuspended in Ham's F-12/M199 medium (1:1, v/v), 5% heat-inactivated fetal bovine serum (experimental medium), and 1% human serum for *in vitro* association and transcytosis assays. The *Cryptococcus* cell number was determined by spectrophotometer at A_{600}. One *A* is equivalent to $\sim 10^8$ B-4500FO2 cells/ml.

Isolation of CD44 from the Membrane Lipid Rafts of HBMEC— The lipid raft fraction was prepared using the caveolae/rafts isolation kit from Sigma (catalog no. CS0750) according to the manufacturer's instruction. Briefly, HBMEC were seeded and grown in a 60-mm Petri dish for 3–4 days and then lysed in 500 μl of Lysis buffer (Sigma, catalog no. L7667) containing a mixture of proteinase inhibitors and 0.5% Triton X-100 on ice and incubated for 30 min on ice. Each sample (0.42 ml) was mixed with 0.58 ml of cold OptiPrep™ from the kit (catalog no. D1556), transferred into an SW40 centrifuge tube, and each overlaid with 1 ml of 30, 25, 20, and 10% OptiPrep™. The gradients were spun at 35,000 rpm in an SW40 rotor for 5 h at 4 °C. Nine fractions (0.5 ml) were collected from the top to the bottom of centrifuge tubes. Fraction 1 from the top was the loading sample in aqueous solution, and fraction 2 was the lipid raft fraction that contained CD44. The hyaluronic acid (HA) assay kit was purchased from Corgenix, Inc. It was used to study the interaction between purified CD44 and coated HA (Fig. 1*B*).

In Vitro Adhesion and Invasion Assays—Immunofluorescence microscopy was used for the *in vitro* adhesion and invasion assays, as described previously (9). The HBMEC were probed with β-actin using a phalloidin-rhodamine conjugate to display a red background. *C. neoformans* C1186 cells stably expressed GFP, which showed a bright green signal under an immunofluorescence microscope in their free form (nonadherent cells). When *C. neoformans* cells adhered to HBMEC, the green signals partially overlapped with the red-stained HBMEC and thus displayed the green/yellow signals (Fig. 4 as an example). The internalized *C. neoformans* cells bearing GFP completely overlapped with red background and thus showed a yellow signal (9). Using this assay, three stages of yeast cell invasion

into HBMEC could be distinguished as follows: nonadherent (bright green), attached/engulfed (green/yellow), and invaded C. neoformans (yellow) cells in HBMEC. For the bikunin (GenScript Corp., catalog no. 300233) studies, HBMEC were pretreated with bikunin for 1 h prior to the adhesion and invasion assays (Fig. 2). The adhered (Fig. 2*A*) or invaded (Fig. 2*B*) *C. neoformans* cells of the untreated controls were designated as 100%, and the effects of siRNA were indicated by the percentage over the control, respectively. For anti-DYRK3 siRNA studies, the green *C. neoformans* signals on the surface of HBMEC (Fig. 8*A*) and the yellow *C. neoformans* signals inside the HBMEC (Fig. 8*B*) were counted under different anti-DRYK3 siRNA treatments as indicated. Five random regions in the chamber slide in each sample were counted. The assay for each experiment was repeated at least three times.

Immunofluorescence Microscopy—Samples for immunofluorescence microscopy were prepared as follows. HBMEC were plated on glass coverslips (22 mm, square), which had been previously coated with type I collagen from rat tail (Upstate, 5–10 μg/cm^2) in an 8-well square culture system (Nalgen Nunc). HBMEC ($1–5 \times 10^3$ cells) were seeded on one coverslip 48–72 h prior to the experiment. HBMEC were prewashed four times with PBS, and then fixed with 2% paraformaldehyde/PBS (v/v) for 30 min at room temperature. After being washed three more times with PBS, the HBMEC were blocked with 5% BSA/PBS for 30 min and then incubated with cholera toxin B (CTxB)-FITC conjugate for 60 min (Sigma, catalog no. C1655, 1–2 μg/ml) and/or an anti-GM3 monoclonal antibody (Cosmo Bio USA, catalog no. NBT-M102, 1:200 dilution) at 4 °C overnight. The coverslips were washed four times with PBS before being sealed onto slides. The anti-CD44 monoclonal antibody (sc 7297) was obtained from Santa Cruz Biotechnology, and the anti-GXM monoclonal antibody (clone 18b7) for staining of *C. neoformans* cell (Fig. 3) was kindly provided by Dr. Casadevall. In some experiments (Fig. 6), HBMEC were pretreated with cytochalasin D (1 μg/ml), nocodazole (5 μg/ml), or anti-DYRK3 siRNA (0–40 pmol as indicated) for 5 h. After changing the medium, the cell cultures were grown overnight and washed again with PBS three times prior to GM1 and GM3 labeling. Samples were examined using the fluorescence microscope at the Congressman Dixon Cellular Imaging Core Facility, Children's Hospital Los Angeles.

In Vitro Transcytosis Assay—C. neoformans in vitro transcytosis assays were performed as described previously (30). Briefly, HBMEC were cultured on collagen-coated transwell polycarbonate tissue culture inserts with a pore diameter of 12 μm (Corning Costar) for 24 h. Triple samples of HBMEC were pretreated with anti-DYRK3 siRNA (10 and 20 pmol in 0.5 ml of culture medium), random oligonucleotides, and mock, individually, for an additional 24 h. HBMEC were polarized to reach a trans-endothelial electrical resistance of 250–300 microohms/cm^2, as measured with an Endohm Volt/Ohm meter (World Precision Instruments). On the morning of the assay, HBMEC monolayers were washed with experimental medium, and 10^6 *Cryptococcus* cells were added to the upper chamber (total volume 500 μl) and then incubated at 37 °C. At 4, 8, and 16 h, samples (100 μl) were taken from the lower chamber and plated to determine CFU. The lower chamber was replenished with 100 μl of fresh culture medium. Simultaneously, the integrity of the HBMEC monolayer was assessed by measurement of the a trans-endothelial electrical resistance. Three measurements were made at each time point for each sample.

siRNA Treatment—Anti-DYRK3 siRNA was purchased from Santa Cruz Biotechnology (sc-39010), and a control oligonucleotide (sc 36869) was used in parallel. Anti-DYRK3 siRNA treatment was performed according to the manufacturer's protocol. LipoD293^{TM} was used as the transfection reagent (catalog no. SL100668, SignaGen Lab, Ijamsville, MD). Briefly, 0–40 pmol of siRNA was transfected into HBMEC. After 5 h, the culture was replaced with fresh medium and grown for 24 h. Then the HBMEC were washed with PBS three times before the experiments. One set of sample was used to detect the DYRK3 protein level (Fig. 7*A*), and another set of treated HBMEC were used for several studies. Similar preparations were performed for immunofluorescence microscopic studies (Fig. 7*B*), *in vitro* invasion assays (Fig. 8), and transcytosis assay (Fig. 9).

Proteomic Studies—The phosphoprotein purification kit (Qiagen, catalog no. 37101) was used. Briefly, HBMEC were cultured in three 100-mm dishes for 2 days until 90% confluent and then transfected with and without anti-DYRK3 siRNA as described above. After 24 h, the cells were collected by scraping in 5 ml of lysis buffer. After 30 min of incubation at 4 °C, the cell lysate was centrifuged, adjusted to 0.1 mg/ml, and applied to the phosphoprotein purification column. After washing with 6 ml of lysis buffer, the phosphoproteins were eluted with 500 μl of elution buffer and concentrated to 50 μl with Nanosep Ultrafiltration columns. The samples were subjected to SDS-PAGE in parallel. The phosphoproteins in anti-DYRK3 siRNA-treated samples were compared with the control, and the marked candidate proteins were identified by LC-MS/MS. Briefly, proteins were separated on a one-dimensional gel and in-gel digested with trypsin as described (31). The resulting peptides were cleaned up using C18 OMIX TIPs (Varian) and analyzed at the Children's Hospital Los Angeles Proteomics Facility using an Eksigent nanoLC-2D coupled to a Thermo Orbitrap XL mass spectrometer, as described previously (32). Proteins were identified based on their tandem mass spectra using Bioworks (Thermo) and Scaffold (Proteome Software) (33) protein identification software packages. All proteins were identified with at least two peptides, with the peptide and protein probabilities of at least 95%, and with cysteine carboxymethylation, methionine oxidation, and STY phosphorylation as variable modifications. For protein blot studies, anti-phospho-filamin A antibody (catalog no. 4761) was purchased from Cell Signaling Technology; anti-filamin antibody (sc 17749) was obtained from Santa Cruz Biotechnology; anti-phospho-dynamin (catalog no. PAI-4621) was acquired from Thermo Scientific; and anti-phospho-Tau antibody (catalog no. 9688) was obtained from Chemicon.

Statistical Analysis—Analysis of variance was performed. The dependent variable was the percent of associated cells or CFU, and the independent fixed factors were the treatments (cytochalasin D, nocodazole, anti-DYRK3 siRNA, or control oligonucleotides). Analysis of variance and analyses of co-variants were followed by the Newman-Keuls multiple comparison test to determine the statistical significance between the control and treatment groups. $p < 0.05$ was considered significant.

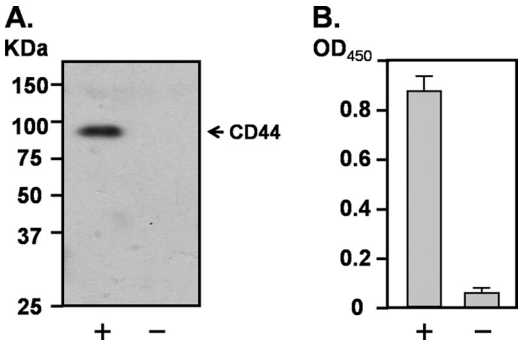

FIGURE 1. **Interaction between lipid raft-associated CD44 and hyaluronic acid.** Aliquots of lipid raft fractions containing CD44 were incubated with HA-coated (+) or mock (−) plates for 60 min. After washing, one set of the samples was eluted for protein blotting with anti-CD44 monoclonal antibody (*A*). Another set was incubated in HA ELISA plate and reacted with anti-CD44-mAb and anti-mouse IgG-HRP conjugate using 3,3′,5,5′-tetramethylbenzidine as the substrate (*B*). The reaction was stopped after 15 min of color development by adding one drop of 0.2 N HCl. Data were obtained from four experiments ($n = 4$).

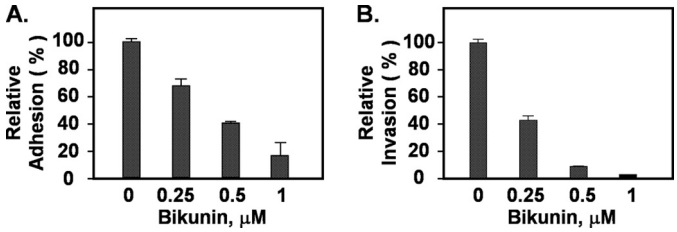

FIGURE 2. **Inhibition of CD44 with bikunin resulting in decreases in both adhesion and invasion of *C. neoformans* to HBMEC.** Adhesion assays (*A*) and invasion assays (*B*) were performed in the presence of 0, 0.25, 0.5, and 1 μM bikunin (GenScript Corp.) without serum in culture medium in a 24-well plate. The total adhered (*A*) or invaded (*B*) *C. neoformans* cells of the untreated samples were designated as 100%. The percentage of *C. neoformans* adhesion or invasion (*y* axis) in cultures containing various amounts of bikunin (*x axis*) was the mean of triplicates ± S.D. from three experiments ($n = 3$).

RESULTS

Molecular Events on the Host Plasma Membrane during C. neoformans Invasion—We have previously shown that the interaction between *C. neoformans* HA and its receptor CD44 plays a key role in the adhesion step (8). However, the precise mechanism had yet to be determined. In this study, we tested whether CD44 molecules isolated from lipid rafts could directly interact with HA. Membrane lipid raft fractions were prepared from HBMEC (8) and then analyzed by ELISA to examine the interaction between HA and CD44 using HA-coated plates to trap CD44. A blank plate was used in parallel as the negative control. After incubation and washing, one set of the samples was eluted for protein blotting analysis (Fig. 1*A*). Another set was assessed by anti-CD44 mAb-HRP conjugate on the ELISA plate, followed by colorimetric measurement (Fig. 1*B*). A single CD44 band of expected size was obtained from the HA-coated plate on the blot but not from the control plate (Fig. 1*A*, *2nd lane*). Similar results were obtained from the HRP colorimetric assay (Fig. 1*B*), demonstrating that there is a direct interaction between lipid raft CD44 and HA. These biochemical results support our hypothesis that the CD44 from lipid rafts can play a role as a host receptor for *C. neoformans*.

Bikunin is a protein in human urine. It can disrupt the oligomerization of CD44 proteins on membrane lipid rafts, resulting in the suppression of receptor-mediated signaling (34). Based on the above information, we addressed the question whether *C. neoformans* invasion activities can be disrupted by bikunin. Using the *in vitro* adhesion and invasion assays, we found that *C. neoformans* adhesion to HBMEC decreased as the concentration of bikunin increased (from 0 to 1 μM) (Fig. 2*A*). Thus, the activation of CD44 (presumably oligomerization on the lipid rafts) in response to cryptococcal cells could be disrupted by bikunin. Similarly, the invasion activity of *C. neoformans* cells was inversely correlated with increased concentrations of bikunin (Fig. 2*B*). This result was as expected as the impairment of adhesion leads to a fewer number of invaded *C. neoformans* cells. Taken together, bikunin abrogated *C. neoformans* adherence to and invasion of HBMEC, presumably due to inhibition of the CD44 function on lipid rafts.

Lipid Raft Marker Ganglioside GM1 Co-localizes with CD44—To further explore the relationship between CD44 and lipid rafts on HBMEC, we used CTxB-FITC conjugate to localize GM1, a marker of lipid rafts. In the fluorescent images, the GM1 signals were observed on the margin of HBMEC, in the plasma membrane. Some intracellular GM1 signals appearing as dotted structures were also observed in the perinuclear regions (Fig. 3*A*, *left panel*). A similar CD44 image was observed (Fig. 3*A*, *right panel*), except that CD44 had a stronger membrane staining. In some cases, a bright spot of GM1 signal near the nucleus, where the peri-centrosomal membrane structures are located, was observed (Fig. 3*B, panel 2*). The CD44 signals were displayed primarily on the plasma membrane (Fig. 3*B, panel 3*). From overlaid images, it was obvious that GM1 and CD44 co-localized on the surface of HBMEC, presumably on the lipid rafts, as observed by the yellow signals (Fig. 3*B, panel 4*). The results suggest that HBMEC CD44 molecules are anchored on the lipid rafts and serve as the host receptor for *C. neoformans*.

C. neoformans Associates with the Lipid Rafts on HBMEC to Establish Its Entry Site—To further examine the role of lipid rafts during *C. neoformans* infection, we examined whether *C. neoformans* could be co-localized with GM1 on the surface of HBMEC. An anti-GXM monoclonal antibody was used to localize *C. neoformans* cells (rhodamine-conjugate, red). In the presence of *C. neoformans*, the signal of GM1 was enhanced (Fig. 4*b*), compared with that without *C. neoformans* cell treatment (Figs. 4*a* and 3*A*). In addition, the bright signals were aligned along the surface of HBMEC at the early stage of *C. neoformans*-host engagement. Images of confocal microscopy showed co-localization of *C. neoformans* cells and GM1 (Fig. 4*c*), as evidenced by the bright yellow region, denoting the site of interaction between the *C. neoformans* cell and the surface GM1 (Fig. 4, *b* and *c*). Taken together, *C. neoformans* cells co-localize with GM1, suggesting that the lipid rafts serve as the portal of *C. neoformans* entry into BMEC.

Influx of Ganglioside GM1 Induced upon C. neoformans Infection—The ganglioside GM1 is a useful marker for lipid rafts, not only on the cell surface but also on the intracellular trafficking of cargo in lipid raft-mediated endocytosis. To explore the lipid raft dynamics, we stained HBMEC with ganglioside GM1 using CTxB-FITC conjugate (green) and GM3 using anti-ganglioside GM3-Ab conjugated with rhodamine

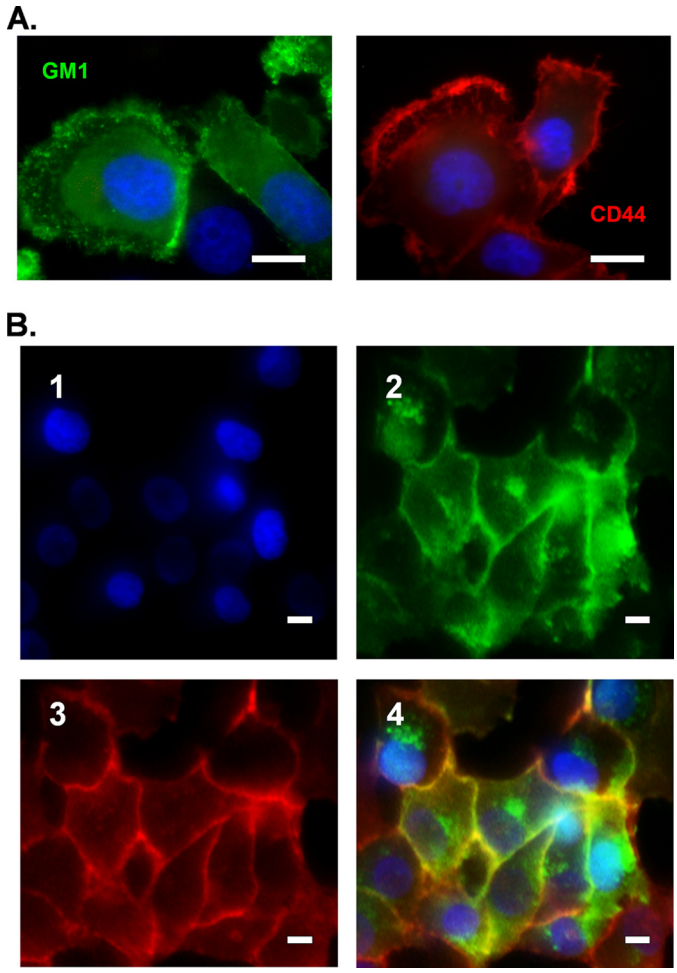

FIGURE 3. **Co-localization of CD44 and the lipid raft marker ganglioside GM1 on the surface of *C. neoformans*-infected HBMEC.** *A,* GM1 (*green*) and CD44 (*red*) localizations were examined by immunofluorescence microscopy. A typical image is shown. *B,* DAPI (*panel 1, blue*) was used to stain nuclear DNA to locate HBMEC. Both GM1 (*panel 2, green*) and CD44 (*panel 3, red*) displayed a clear membrane staining pattern. An overlaid image is shown in *panel 4*. *Bar,* 20 μm.

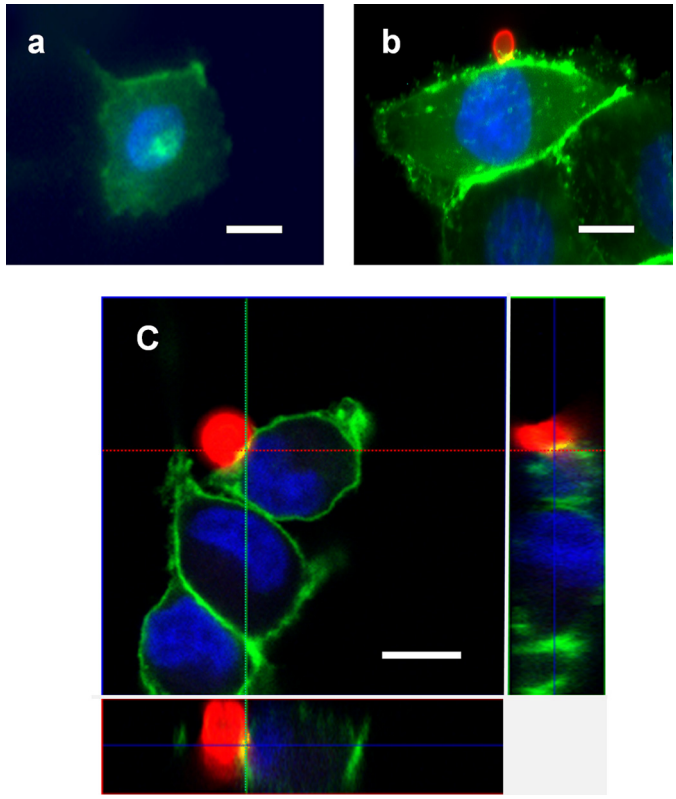

FIGURE 4. **Association of *C. neoformans* associates with the lipid rafts of HBMEC to establish a *C. neoformans* entry site.** *a,* HBMEC was stained with CTxB-FITC conjugate as the control. *b, C. neoformans* (*red*) and lipid raft GM1 (*green*) were co-localized on the surface of HBMEC during the *C. neoformans* infection. *C. neoformans* was stained with anti-GXM mAb and anti-mouse IgG-rhodamine conjugate. *c,* confocal microscopy was performed to examine adhered *C. neoformans* cells (*red*, anti-GXM mAb), HBMEC membrane (*green*, CTxB-FITC), and HBMEC nuclear DNA (*blue*, DAPI). Two side view sections are displayed on the *right* and *below* the main image. *Bar,* 20 μm.

conjugated (red), followed by staining nuclear DNA (blue) with DAPI as the nuclear marker. Both gangliosides GM1 and GM3 are essential components of cellular membrane systems. Because they differ in distribution and dynamics, they were examined side by side as the controls against each other. In general, GM3 (red) staining was seen around the perinuclear regions in the cytosol without co-localization with the DAPI staining (Fig. 5). Its signals were covered, not co-localized, by those of GM1 (green) (Fig. 5*A*, *stages 1* and *2*), and the red signal (GM3) became more intense when GM1 signals were diminished (Fig. 5*A*, *stages 3* and *4*). In contrast, the GM1 stains were quite dynamic and could be generalized into four different stages during *C. neoformans* infection. In the absence of *C. neoformans*, the GM1 stains appeared on the plasma membrane and, to a lesser extent, in some intracellular regions (Fig. 5, *stage 0*). In the presence of *C. neoformans*, the GM1 signals became much brighter and were clustered on the surface of HBMEC (Fig. 5, *stage 1*). Upon prolonged incubation with *C. neoformans* (>30 min), some GM1 stains were invaginated into the plasma membrane and accumulated in large vesicular structures (presumably endosomes) throughout the cytosol (Fig. 5, *stage 2*). With further incubation (~60 min), the GM1 staining retracted to the nucleus and co-localized with the DAPI staining, *i.e.* green staining co-localized with blue DAPI staining showing a white/bluish signal on the nucleus (Fig. 5, *stage 3*). Eventually, little or no green signal was observed in the cytosol (Fig. 5, *stage 4*). In a 1-h incubation period with *C. neoformans*, ~20% of the HBMEC had white nuclear stains (Fig. 5, *stages 3* and *4*). The GM3 (red) staining was still around the nucleus but slightly expanded outwards, probably due to the fact that the GM3 signal could be easily detected in the absence of GM1 signals (Fig. 5, *stage 3* and *4*). The movement of GM1, but not that of GM3, appears to be specific to *C. neoformans* infection. GM1 dynamics were not observed in HBMEC infected with other pathogens such as *E. coli* (data not shown). Because GM1 is a widely used lipid raft marker to explore endocytic pathways in different cell types, the data lead us to believe that *C. neoformans* may activate the GM1-linked endocytic pathway.

We then used confocal microscopy to examine this unique cellular effect. A *C. neoformans* infected HBMEC cell was scanned from top to bottom with 1 μm in each section (supplement Fig. S1). A central section with both GM1 and DAPI stains is shown in Fig. 5*B*. Two side view images, reconstituted by the ScanLine program, are shown on the *upper* and *right sides* of Fig. 5*B*. From these images, it was clear that GM1 was able to

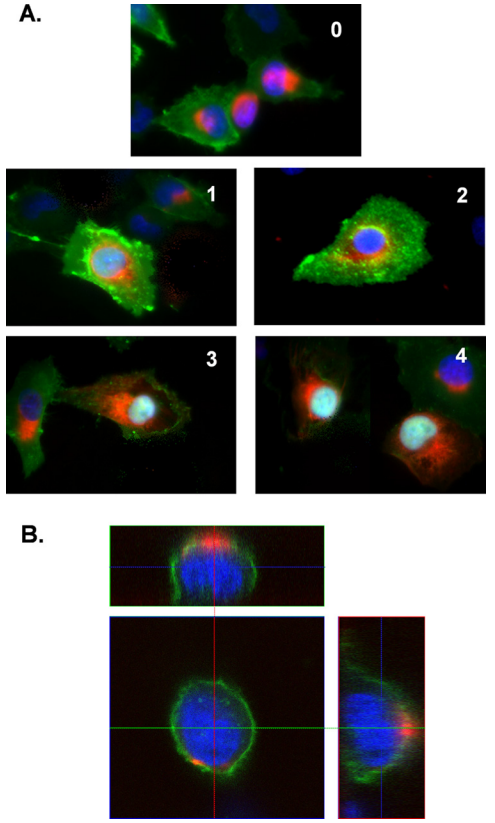

FIGURE 5. **Influx of ganglioside GM1 during *C. neoformans* infection.** *A,* distribution of gangliosides GM1 (*green*) and GM3 (*red*) during *C. neoformans* infection is shown. HBMEC without *C. neoformans* treatment was used as the control (*stage 0*); other images were selected to represent different *stages 1–4* of GM1 and GM3 distributions. *B,* confocal microscopy was performed to dissect an HBMEC image, 1 μm per section. A middle section is shown. Two side view images are displayed on the *top* and *right* of the main image. A complete set of confocal microscopic sections is shown in supplemental Fig. S1.

migrate and concentrate itself on the nuclear membrane during *C. neoformans* infection, seen as a white/bluish signal inside HBMEC (supplement Fig. S1).

C. neoformans-induced Endocytic Dynamics Require Actin Filaments, Microtubules, and DYRK3—Endocytosis is regulated by a number of kinases and has been shown to be blocked by the actin depolymerization reagent, cytochalasin D, and the microtubule-stabilizing reagent, nocodazole, in CHO cells (35). We therefore tested the effects of cytochalasin D, nocodazole, and anti-DYRK3 siRNA on the distribution of GM1 inside HBMEC induced by *C. neoformans*. In the absence of inhibitors, *C. neoformans* enhanced GM1 (CTxB-FITC) signals (stage 1, ~25%) and promoted the formation of vesicular structures inside HBMEC (stage 2, ~40%) with ~15% "white" nuclei present in stage 3 and 4 (Fig. 6). However, in the presence of either cytochalasin D or nocodazole, the influx of GM1 was significantly inhibited, and more than 60% of HBMEC remained in stage 1 with few white/bluish nuclei being observed. The results suggested that the movement of the intracellular vesicles of endocytic machinery was blocked by either cytochalasin D or nocodazole. Thus, the cytoskeletal machinery was required for the endocytotic routes, induced by *C. neoformans*, in HBMEC. Both cytochalasin D (9) and nocodazole were also found to block *C. neoformans* invasion into HBMEC in a dose-dependent manner (data not shown).

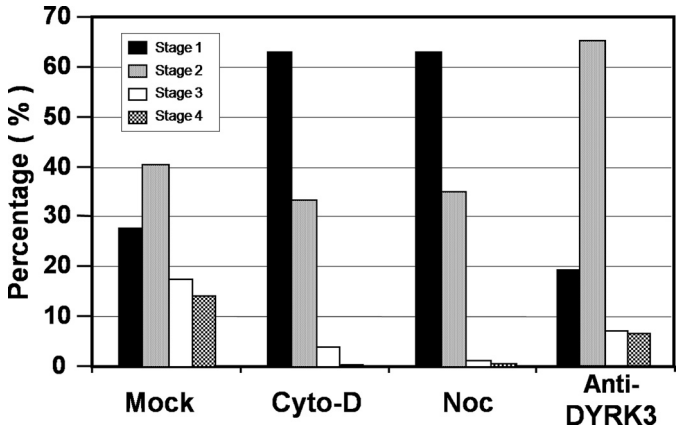

FIGURE 6. **Cytochalasin D, nocodazole, or anti-DYRK3 siRNA treatment can reduce the influx of GM1 in HBMEC.** Immunofluorescence microscopy was performed to examine GM1 distribution in different stages as mentioned in the legend of Fig. 5. HBMEC were pretreated with mock, cytochalasin D (*Cyto-D*), or nocodazole (*Noc*) for 1 h and washed three times with PBS before *C. neoformans* incubation. For the third set of samples, HBMEC were transfected with anti-DYRK3 siRNA for 24 h, prior to *C. neoformans* incubation. Images of different stages were obtained from 1 h of incubation. Each number was the average of four different slides ($n = 4$).

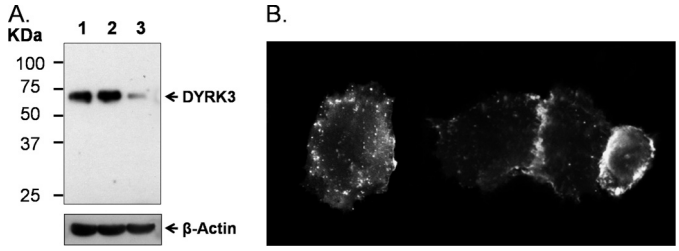

FIGURE 7. **Effect of anti-DYRK3 on GM1 redistribution in HBMEC.** *A,* protein blot shows the DYRK3 level in HBMEC treated with mock (*lane 1*), random oligonucleotide control (*lane 2*), and anti-DYRK3 siRNA treatment (20 pmol) (*lane 3*). Anti-DYRK3 antibody was used to detect the DYRK3 proteins (*upper panel*), and antibody against β-actin was used as the loading control (*bottom panel*). *B,* CTxB-FITC was used to stain GM1 of HBMEC. The immunofluorescence microscopic image shows the terminal phenotype of DYRK3 knockdown in HBMEC, *i.e.* accumulation of vesicular structures throughout the cytosol.

DYRK3 is a dual specificity tyrosine phosphorylation-regulated kinase. The DYRK3 knockdown phenotype in HeLa cells is very similar to the stage 2 morphology of HBMEC, as shown in Fig. 5 (also see below). Therefore, we examined whether DYRK3 was functional in HBMEC. After 24 h of DYRK3 siRNA treatment, one set of samples was used to determine the DYRK3 protein level (Fig. 7*A*). Under our experimental conditions, >60% of endogenous DYRK3 protein was knocked down in the anti-DYRK3 siRNA-treated HBMEC (Fig. 7*A*, *lane 3*) compared with the controls (Fig. 7*A*, *lanes 1* and *2*). Another set of samples was examined under an immunofluorescence microscope to determine the DYRK3 knockdown phenotype in HBMEC, and the images showed that DYRK3 was primarily located in the cytosol of HBMEC, which might represent the untransfected HBMEC in the pool. The signals were diminished in the presence of anti-DYRK3 siRNA (data not shown). When anti-DYRK3 siRNA-treated HBMEC were stained with CTxB-FITC, GM1 in many cells was found to be located inside the cells, as shown by dense vesicular structures in the cytosol similar to those seen in stage 2. A typical morphology of anti-DYRK3 siRNA-treated HBMEC is shown in Fig. 7*B*. There were

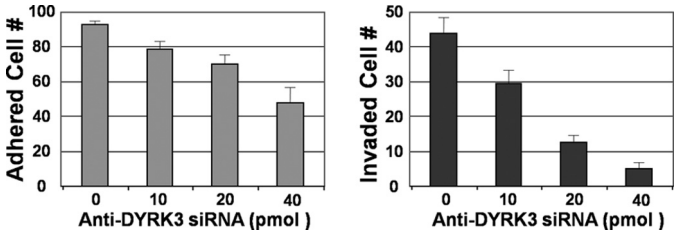

FIGURE 8. **Effect of DYRK3 knockdown on *C. neoformans* adhesion to and invasion of HBMEC.** HBMEC were pretreated with 10, 20, and 40 pmol of anti-DYRK3 siRNA in the chamber slide well (0.2 ml) before adhesion and invasion analyses. Each *bar* represents the average of three different experiments ± S.D. ($n = 3$).

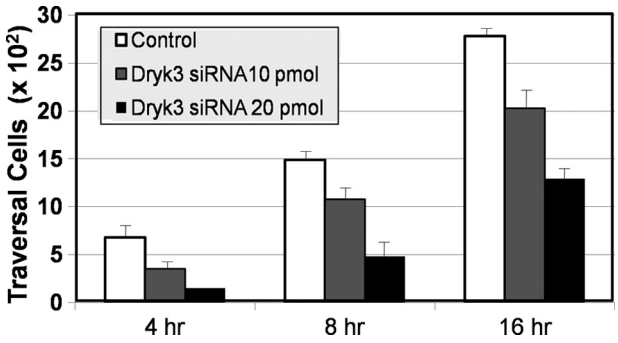

FIGURE 9. **Effect of DYRK3 on *C. neoformans* transversal across the blood-brain barrier *in vitro*.** HBMEC (10^4 cells) were seeded on a collagen-coated transwell for 4 days, until transendothelial electric resistance reached >250 micro-ohms/cm^2. The coated cultures were treated with control oligonucleotide (sc 36869) or anti-DYRK3 siRNA (sc 39010), either 10 or 20 pmol in the 0.5-ml upper chamber, for 24 h before the transcytosis study. CFU was determined from the culture in the lower chamber of the transwell, and the recovery percentage was determined at 4, 8, and 16 h ($n = 3$). Analysis of variance shows a significant decrease in transcytosis in the DYRK3 knockdown in HBMEC at every time point ($p = 0.015$).

some GM1 signals in the connecting regions between two cells, but the large dense vesicles were distributed throughout the cell. Some cells exhibited strong membrane staining, probably because of an incomplete DYRK3 knockdown, as seen in Fig. 7*B*. Greater than 60% of anti-DYRK3 siRNA-treated cells showed a predominant stage 2 phenotype (Fig. 6, *4th column*). This finding, along with the studies of cytochalasin D and nocodazole, showed that *C. neoformans*-induced GM1 redistribution can be blocked by endocytosis inhibitors.

Effect of Anti-DYRK3 siRNA on C. neoformans Adhesion, Invasion, and Traversal across the HBMEC Monolayer—To determine whether DYRK3 function is linked to *C. neoformans* invasion, we examined whether *C. neoformans* invasion is affected by DYRK3 knockdown in HBMEC by immunofluorescence microscopy (9). *C. neoformans* strain C1186 was used because the cells express a stable green fluorescence protein (GFP). HBMEC were stained for intracellular β-actin using phalloidin-rhodamine conjugate. The adhered *C. neoformans* cell showed a green/yellow signal on the surface of HBMEC (Fig. 4 as example), and the invaded *C. neoformans* cells in HBMEC exhibited a yellow signal when the green *C. neoformans* cell co-localizes with the intracellular red actin signals (see "Experimental Procedures"). HBMEC samples were pretreated with different amounts of anti-DYRK3 siRNA. The results showed that the levels of *C. neoformans* adhesion and, to a larger extent, invasion into HBMEC was inversely proportional to the concentration of anti-DYRK3 siRNA used (Fig. 8).

We then performed an *in vitro* transcytosis assay to examine the ability of *C. neoformans* across the HBMEC monolayer. The results showed that the ability of *C. neoformans* to traverse across the monolayer was decreased in the cells transfected with anti-DYRK3 siRNA (Fig. 9*B*). This observation suggests that DYRK3 is involved in *C. neoformans* internalization into HBMEC, presumably mediated by the endocytic pathway.

DISCUSSION

We have previously demonstrated that the interaction between *C. neoformans* HA and HBMEC CD44 initiates *C. neoformans* brain invasion (6–8). These results support the hypothesis that *C. neoformans* traverses the blood-brain barrier following a "transcellular pathway." A scanning electron microscopic study has shown that microvilli and membrane extension embraced *C. neoformans* during its internalization, suggesting that *C. neoformans* invasion of HBMEC utilizes a "zipper-like mechanism" in which the host cell plasma membrane enwraps the invading yeast (36). This mechanism therefore requires *C. neoformans* cell-induced HBMEC cytoskeletal rearrangements to accumulate actin fibers at the site of *C. neoformans* entry. The *C. neoformans* cell is then drawn into the host cell. However, the molecular nature of this process has not been demonstrated. Because the entry process of *C. neoformans* could be abolished by filipin, which extracts cholesterol from the membrane lipid rafts (8), we hypothesize that the membrane lipid rafts that mediate endocytosis are involved in the process of invading *C. neoformans*. In this study, we first demonstrated that CD44 molecules isolated from lipid rafts can directly interact with hyaluronic acid (Fig. 1). Also, the CD44 function can be blocked by bikunin, presumably by perturbation of its oligomerization on the lipid rafts (Fig. 2). We then used CTxB-FITC to monitor the lipid raft marker GM1 dynamics (Figs. 3–5) and made several novel findings.

First, the *C. neoformans* cell co-localizes with GM1 on the surface of HBMEC, presumably the entry site into *C. neoformans* (Fig. 4). The results support our previous hypothesis that HA and HBMEC CD44 of *C. neoformans* play a crucial role during *C. neoformans* infection (7, 8). This may be an essential step in the successful colonization and development of disease by *C. neoformans*. The ability to adhere to the host cell surfaces is conceivably crucial for withstanding the blood flow *in vivo*. Our results suggest that internalization of *C. neoformans* takes place on the surface lipid rafts of HBMEC.

It is known that lipid raft formation and/or stabilization are highly regulated and occur only in response to stimulation, such as receptor clustering. Lipid rafts in unstimulated cells are small and unstable, if they exist at all. However, clustering of molecules with high affinity for ordered lipids greatly increases raft size and stability (37). Thus, the clustering of cell surface receptors, as often occurs during signaling, may increase the affinity of the clustered receptors and may also stabilize or further induce lipid raft formation. Upon *C. neoformans* engagement, the GM1 signal was found to be significantly increased (Figs. 4 and 5), suggesting that a microdomain organization assembles a signaling network on the plasma membrane. In

addition to its roles on the plasma membrane, lipid rafts also play key roles in membrane trafficking.

Second, *C. neoformans* induces a significant redistribution of GM1 on the nuclear membrane. It is well known that GM1 is present on the plasma membrane and intracellular endosome membrane systems, and it may accumulate in perinuclear regions, such as Golgi apparatus and peri-centrosomal regions (22, 23). To our knowledge, this is the first demonstration of nuclear membrane localization of GM1 induced by *C. neoformans* (Fig. 5*B* and supplement Fig. S1). One possible reason for our novel finding is that our images were counterstained with GM3 (red) to generate a white/bluish signal that is more easily identified. Another possibility is that GM1 distribution to the nuclear membrane is specific to HBMEC. The efficient trafficking of GM1 by the lipid raft-mediated endocytosis appears to be dependent upon intact actin filaments, the microtubule cytoskeleton (35), and the DYRK3 kinase (Fig. 6). We have dissected the *C. neoformans*-induced endocytic process into 4 stages (Fig. 5*A*). These unique HBMEC phenotypes may be useful for screening the many *C. neoformans* mutants that exist (38).

Third, DYRK3 is required for GM1 intracellular trafficking, and knockdown of DYRK3 affects the invasion and transcytosis of *C. neoformans* across HBMEC (Figs. 8 and 9). Currently, little is known regarding the exact biological functions of DYRK3. The clue for its involvement in *C. neoformans* invasion comes from the genome-wide screening of human kinases, showing that the lipid raft endocytic route is regulated by a specific kinase subset. One group of kinases (DYRK3, VRK1, and DTYMK) has been shown to exert their effects on GM1 redistribution during SV40 infection in HeLa cells (29, 39). Interestingly, we found that GM1 redistribution takes place during *C. neoformans* infection. One obvious phenotype (*stage 2,* Fig. 5*A*) is that many CTxB-stained intracellular vesicular structures were observed in the anti-DYRK3 siRNA-treated HBMEC; presumably, in the absence of DYRK3, the plasma membrane GM1 was internalized and trapped as enlarged vesicular structures of endocytic machinery inside the HBMEC (Fig. 7*B*). A similar morphology was observed in the DYRK3-knockdown HeLa cells (29). We have found that knockdown of DYRK3 abolishes phosphorylation of filamin A in HBMEC (see supplement Fig. S2), suggesting that filamin A is a potential substrate (or a downstream effector) of DYRK3. It is well documented that filamin A is involved in endocytosis (40–44). Thus, our results generated from HBMEC are consistent with those from HeLa cells, supporting the notion that DYRK3 is involved in the endocytic pathway.

Although both SV40 and *C. neoformans* induce the formation of vesicular structures in the cytosol (stage 2 phenotype), it is important to note that SV40 viruses usually traffic through caveosomes to the endoplasmic reticulum before being transported to the nucleus for replication. But *C. neoformans* cells may use the endocytic route for internalization and then continue to cross the HBMEC monolayer. Thus, there are differences and similarities regarding how viruses and *C. neoformans* use the host endocytic pathway for invasion. Based on results of DYRK3 knockdown studies, we believe that DYRK3 plays a direct role on GM1 redistribution through a lipid raft-mediated endocytosis. Our demonstration that *C. neoformans* uses the endocytic signaling of HBMEC traversal of the monolayer may provide a clue for novel treatments of *C. neoformans* infection. Several pharmacological reagents can be used to block the endocytic pathway such as statins (lovastatin, simvastatin, and pravastatin), filipin, nystatin, and cholesterol oxidase (45). In fact, treating HBMEC with filipin have been shown to block *C. neoformans* invasion (8).

DYRK3 was first identified as the kinase that negatively regulated erythropoiesis (46, 47). How do our results reconcile with its roles in erythropoiesis? One possible explanation is that DYRK3 plays different roles in different cell types. Because endocytosis supports a wide range of cellular functions, including nutrient uptake, regulation of growth factors, cell-surface homeostasis, and synaptic transmission, DYRK3 may be required for transporting signaling protein(s) through the endocytic route to regulate erythropoiesis. DYRK3 has been shown that it is required for trafficking of some factors, which participate in cyclic AMP-response element-binding protein transcription (28). Therefore, the roles of DYRK3 in erythropoiesis may be indirect, mediating through endocytic trafficking of some factors to regulate the erythropoiesis. We believe that DYRK3 plays a direct mechanistic role in endocytosis (Figs. 6 and 7 and supplement Fig. S2). The lack of DYRK3 function may prevent the cycling of cargo vesicles, resulting in enlarged vesicular structures in the cytosol of HBMEC.

In summary, our novel observations in this study include the following. First, infection of *C. neoformans* increases the activities of lipid rafts on the surface of endothelial cells. Second, GM1 translocates from membrane lipid rafts to the perinuclear membrane upon *C. neoformans*; this may affect lipid raft sorting, trafficking, and positioning through the endocytic pathway. Third, DYRK3 is required for *C. neoformans* invasion, suggesting that *C. neoformans* may use the endocytic signaling pathway in HBMEC to facilitate its invasion. Studies of cytochalasin D and nocodazole on GM1 dynamics also support this notion. Further studies of the host endocytic pathway is necessary to obtain a clearer picture on how *C. neoformans* traverses across the blood-brain barrier.

Acknowledgments—We thank Jennifer Liu for critical reading of this manuscript and Dr. Casadevall for providing the anti-GXM monoclonal antibody.

REFERENCES

1. Kwon-Chung, K. J., and Bennett, J. E. (1978) *Am. J. Epidemiol.* **108,** 337–340
2. Casadevall, A., and Pirofski, L. (2001) *J. Infect. Dis.* **184,** 337–344
3. Park, B. J., Wannemuehler, K. A., Marston, B. J., Govender, N., Pappas, P. G., and Chiller, T. M. (2009) *AIDS* **23,** 525–530
4. Zaragoza, O., Rodrigues, M. L., De Jesus, M., Frases, S., Dadachova, E., and Casadevall, A. (2009) *Adv. Appl. Microbiol.* **68,** 133–216
5. Rubin, L. L., and Staddon, J. M. (1999) *Annu. Rev. Neurosci.* **22,** 11–28
6. Chang, Y. C., Jong, A., Huang, S., Zerfas, P., and Kwon-Chung, K. J. (2006) *Infect. Immun.* **74,** 3930–3938
7. Jong, A., Wu, C. H., Chen, H. M., Luo, F., Kwon-Chung, K. J., Chang, Y. C., Lamunyon, C. W., Plaas, A., and Huang, S. H. (2007) *Eukaryot. Cell* **6,** 1486–1496
8. Jong, A., Wu, C. H., Shackleford, G. M., Kwon-Chung, K. J., Chang, Y. C., Chen, H. M., Ouyang, Y., and Huang, S. H. (2008) *Cell. Microbiol.* **10,** 1313–1326

9. Jong, A., Wu, C. H., Prasadarao, N. V., Kwon-Chung, K. J., Chang, Y. C., Ouyang, Y., Shackleford, G. M., and Huang, S. H. (2008) *Cell. Microbiol.* **10,** 1854–1865
10. Lajoie, P., and Nabi, I. R. (2007) *J. Cell. Mol. Med.* **11,** 644–653
11. Nabi, I. R., and Le, P. U. (2003) *J. Cell Biol.* **161,** 673–677
12. Parton, R. G., and Richards, A. A. (2003) *Traffic* **4,** 724–738
13. Nichols, B. (2003) *J. Cell Sci.* **116,** 4707–4714
14. Nichols, B. J., Kenworthy, A. K., Polishchuk, R. S., Lodge, R., Roberts, T. H., Hirschberg, K., Phair, R. D., and Lippincott-Schwartz, J. (2001) *J. Cell Biol.* **153,** 529–541
15. Lafont, F., and van der Goot, F. G. (2005) *Cell. Microbiol.* **7,** 613–620
16. Seveau, S., Bierne, H., Giroux, S., Prévost, M. C., and Cossart, P. (2004) *J. Cell Biol.* **166,** 743–753
17. Yavlovich, A., Tarshis, M., and Rottem, S. (2004) *FEMS Microbiol. Lett.* **233,** 241–246
18. Pelkmans, L., and Helenius, A. (2002) *Traffic* **3,** 311–320
19. Pelkmans, L., Püntener, D., and Helenius, A. (2002) *Science* **296,** 535–539
20. Pelkmans, L. (2005) *Curr. Opin. Microbiol.* **8,** 331–337
21. Pelkmans, L., and Helenius, A. (2003) *Curr. Opin. Cell Biol.* **15,** 414–422
22. Lencer, W. I., and Tsai, B. (2003) *Trends Biochem. Sci.* **28,** 639–645
23. Chinnapen, D. J., Chinnapen, H., Saslowsky, D., and Lencer, W. I. (2007) *FEMS Microbiol. Lett.* **266,** 129–137
24. Guo, X., Williams, J. G., Schug, T. T., and Li, X. (2010) *J. Biol. Chem.* **285,** 13223–13232
25. Becker, W., Weber, Y., Wetzel, K., Eirmbter, K., Tejedor, F. J., and Joost, H. G. (1998) *J. Biol. Chem.* **273,** 25893–25902
26. Lord, K. A., Creasy, C. L., King, A. G., King, C., Burns, B. M., Lee, J. C., and Dillon, S. B. (2000) *Blood.* **95,** 2838–2846
27. Bogacheva, O., Bogachev, O., Menon, M., Dev, A., Houde, E., Valoret, E. I., Prosser, H. M., Creasy, C. L., Pickering, S. J., Grau, E., Rance, K., Livi, G. P., Karur, V., Erickson-Miller, C. L., and Wojchowski, D. M. (2008) *J. Biol. Chem.* **283,** 36665–36675
28. Li, K., Zhao, S., Karur, V., and Wojchowski, D. M. (2002) *J. Biol. Chem.* **277,** 47052–47060
29. Pelkmans, L., Fava, E., Grabner, H., Hannus, M., Habermann, B., Krausz, E., and Zerial, M. (2005) *Nature* **436,** 78–86
30. Chen, S. H., Stins, M. F., Huang, S. H., Chen, Y. H., Kwon-Chung, K. J., Chang, Y., Kim, K. S., Suzuki, K., and Jong, A. Y. (2003) *J. Med. Microbiol.* **52,** 961–970
31. Shevchenko, A., Tomas, H., Havlis, J., Olsen, J. V., and Mann, M. (2006) *Nat. Protoc.* **1,** 2856–2860
32. Berndsen, C. E., Tsubota, T., Lindner, S. E., Lee, S., Holton, J. M., Kaufman, P. D., Keck, J. L., and Denu, J. M. (2008) *Nat. Struct. Mol. Biol.* **15,** 948–956
33. Sadygov, R. G., Cociorva, D., and Yates, J. R., 3rd (2004) *Nat. Methods* **1,** 195–202
34. Wakahara, K., Kobayashi, H., Yagyu, T., Matsuzaki, H., Kondo, T., Kurita, N., Sekino, H., Inagaki, K., Suzuki, M., Kanayama, N., and Terao, T. (2005) *J. Cell. Biochem.* **94,** 995–1009
35. Mundy, D. I., Machleidt, T., Ying, Y. S., Anderson, R. G., and Bloom, G. S. (2002) *J. Cell Sci.* **115,** 4327–4339
36. Chang, Y. C., Stins, M. F., McCaffery, M. J., Miller, G. F., Pare, D. R., Dam, T., Paul-Satyaseela, M., Kim, K. S., Kwon-Chung, K. J., and Paul-Satyasee, M. (2004) *Infect. Immun.* **72,** 4985–4995
37. Kusumi, A., and Suzuki, K. (2005) *Biochim. Biophys. Acta* **1746,** 234–251
38. Moyrand, F., Fontaine, T., and Janbon, G. (2007) *Mol. Microbiol.* **64,** 771–781
39. Pelkmans, L., and Zerial, M. (2005) *Nature* **436,** 128–133
40. Popowicz, G. M., Schleicher, M., Noegel, A. A., and Holak, T. A. (2006) *Trends Biochem. Sci.* **31,** 411–419
41. Sverdlov, M., Shinin, V., Place, A. T., Castellon, M., and Minshall, R. D. (2009) *Mol. Biol. Cell* **20,** 4531–4540
42. Fiori, J. L., Zhu, T. N., O'Connell, M. P., Hoek, K. S., Indig, F. E., Frank, B. P., Morris, C., Kole, S., Hasskamp, J., Elias, G., Weeraratna, A. T., and Bernier, M. (2009) *Endocrinology* **150,** 2551–2560
43. Cho, E. Y., Cho, D. I., Park, J. H., Kurose, H., Caron, M. G., and Kim, K. M. (2007) *Mol. Endocrinol.* **21,** 2242–2254
44. Seck, T., Baron, R., and Horne, W. C. (2003) *J. Biol. Chem.* **278,** 10408–10416
45. Ivanov, A. I. (2008) *Methods Mol. Biol.* **440,** 15–33
46. Wojchowski, D. M., Menon, M. P., Sathyanarayana, P., Fang, J., Karur, V., Houde, E., Kapelle, W., and Bogachev, O. (2006) *Blood Cells Mol. Dis.* **36,** 232–238
47. Zhang, D., Li, K., Erickson-Miller, C. L., Weiss, M., and Wojchowski, D. M. (2005) *Genomics* **85,** 117–130